High Frequency Impedance Analysis for Sensorless Starting of Wound Rotor Synchronous Machines

Andreea Beciu, Emmanuel Godoy, Pedro Rodriguez-Ayerbe, Imen Bahri, Amira Maalouf

High Frequency Impedance Analysis for Sensorless Control of Wound Rotor Synchronous Machines

First A. Author [*,**] **First A. Author** [*] **First A. Author** [*]
Second B. Author, Jr. [**] **Third C. Author** [***]

[*] *Laboratoire des signaux et systmes L2S, UMR CNRS 8506, CentraleSupélec-CNRS-Université Paris Saclay, Gif-sur-Yvette, France (e-mail: Andreea.Beciu@centralesupelec.fr, Emmanuel.Godoy@centralesupelec.fr, Pedro.Rodriguez@centralesupelec.fr).*
[**] *GEEPS - Group of electrical engineering, Paris, Gif-sur-Yvette, France, (e-mail: Imen.Bahri@centralesupelec.fr)*
[***] *Thales-AES, 41 Bvd. de la République, 78400, Chatou, France (e-mail: Amira.Maalouf@fr.thalesgroup.com)*

Abstract: In sensorless control for synchronous machines at low speed and standstill, the position estimation can be sensible to the choice of the carrier frequency of the injection method. Moreover, in presence of saturation or temperature variation, the frequency dependent error is evolving. In order to better describe the high-frequency behaviour of the machine, the effective inductances and resistances are calculated. The analytical expression for the carrier frequency dependent phase delay, is explained using the HF-equivalent model and is proposed to be integrated into the sensorless control schema when a rotating high frequency voltage injection (HFIR) is employed. Numerical simulations highlight the frequency dependent phase delay and prove the satisfactory operation of the compensation.

Keywords: Sensorless control, Wound Rotor Synchronous Machine, Estimation, Impedance, Dumper winding, Saturation – Five to ten keywords, preferably chosen from the IFAC keyword list: Estimation and filtering, Engine modelling and control, Avionics and on-board equipments, Simulation

1. INTRODUCTION

In the context of the more electric aircraft, the brushless exciter synchronous starter/generators (BESSG) are known for their ability to provide high torque during the starting phase of their associated reactor. Due to their proximity to reactors, position sensors have to be able to support very high temperatures (over $250°C$) so they increase costs, complexity and their behaviour in case of failure rises a problem of security.

However, precise knowledge of the rotor position is essential for field oriented control (FOC) of the main engine, a wound rotor synchronous machines (WRSM) with damping windings. The difficulty to suppress position sensors is that the position is not observable at standstill and very low speed. For salient machines, the use of high frequency carrier injection methods to estimate the rotor position is possible because the injected stator or rotor currents provide the system's observability Koteich et al. (2015). Implementation of sensorless control methods using rotating or pulsating high frequency carrier injection on a WRSM can be found in Maalouf et al. (2011) and respectively Griffo et al. (2012); Rambetius and Piepenbreier (2014).

Recent methods of estimation have been proposed in literature that require a high frequency signal to be injected into the rotor winding Koteich et al. (2015); Rambetius and Piepenbreier (2014); Choi et al. (2013). This methods cannot be directly applied to a BESSG because the rotor current cannot be measured or mechanically approached due to the structure of the machine Maalouf et al. (2011). However, another approach for this architecture is to use the exciter stator current harmonics as carrier signals instead of the harmonics of a carrier frequency injection to determine the rotor position Markunas and Romenesko (2006); Kato and Nishikata (2009).

The analysis presented in this paper treats rotating high frequency carrier injection on a WRSM with damper circuits. The sole application of an injection algorithm is not sufficient for a proper estimation. The integrity of the demodulated signal that contains the position dependent harmonics is essential because all distortions are accumulated and reflected as a bias or an oscillation over the estimated signal. In this context, signal processing and phase delays compensation play an important role in

⋆ Sponsor and financial support acknowledgment goes here. Paper titles should be written in uppercase and lowercase letters, not all uppercase.

the structure of the observer. Factors that can introduce phase delays and distortions :

- Architecture and characteristics of the machine: the presence of secondary saliencies, saturation and cross-saturation effects Rambetius et al. (2014); El-Serafi et al. (1988); El-Serafi and Abdallah (1992); Chedot et al. (2007); Raca et al. (2008); Reigosa et al. (2010)
- Signal processing delays Mansouri-Toudert et al. (2013), distortions caused by the current loop Briz et al. (2000); Ovrebo (2004); Garcia et al. (2006).
- Dead-time and non-ideal inverter characteristics Raca et al. (2008); Garcia et al. (2006).

The performances of the HF-injection methods are dependent on the characteristics of the saliency of each studied machine. The aim of this paper is to find a HF-saliency model for a WRSM with damper circuits and give an insight over the estimation errors taking into account the excitation frequency and parameter evolution. A compensation schema is proposed and its efficiency is supported by numerical simulations.

The paper is organised as follows: section II is dedicated to the electrical and mechanical equations of the machine taking into account the magnetic saturation and a simplified high frequency model is further proposed; section III presents the principle of rotating high frequency carrier injection and analyses the influence of the saturation in the high frequency model; section IV deals with the estimation of the position using a tracking observer and phase compensation, the paper is concluded with simulation results and final remarks.

2. MODEL OF THE WRSM

In this section, the main engine of the BESSG is modelled as a WRSM with damper windings. The damper windings are modelled by two shorted circuits on the d and q axis respectively. It has been shown that short-circuited windings contribute to the electromagnetic saliency and that they interact with the HF test-signal Graus and Hahn (2014). In order to better describe the HF-behaviour of the machine, the effective inductances and resistances will be further calculated.

All the rotor parameters are referred to the stator and marked by a prime symbol ($'$). A complete description of the model and corresponding relationships to a model in the natural frame can be found in Barakat et al. (2010). The Park transformation from three-phase to $d-q$ reference frame is used in order to obtain the electrical equations under the classical assumptions :

$$\begin{cases} v_d = R_s.i_d + \frac{d\psi_d}{dt} - \omega_e\psi_q \\ v_q = R_s.i_q + \frac{d\psi_q}{dt} + \omega_e\psi_d \\ v'_f = R'_f.i'_f + \frac{d\psi'_f}{dt} \\ 0 = R'_D.i'_D + \frac{d\psi'_D}{dt} \\ 0 = R'_Q.i'_Q + \frac{d\psi'_Q}{dt} \end{cases} \quad (1)$$

Under the assumption that the inductances on the d-axis are decoupled from those on q-axis (no cross-saturation terms are taken into account), the flux linkage relationship to currents is described by the following matrix products, eq. (2, 3).

$$\begin{bmatrix} \psi_d \\ \psi'_f \\ \psi'_D \end{bmatrix} = \begin{bmatrix} L_d & L_{ad} & L_{ad} \\ L_{ad} & L'_f & L_{ad} \\ L_{ad} & L_{ad} & L'_D \end{bmatrix} \begin{bmatrix} i_d \\ i'_f \\ i'_D \end{bmatrix} \quad (2)$$

$$\begin{bmatrix} \psi_q \\ \psi'_Q \end{bmatrix} = \begin{bmatrix} L_q & L_{aq} \\ L_{aq} & L'_Q \end{bmatrix} \begin{bmatrix} i_q \\ i'_Q \end{bmatrix} \quad (3)$$

Motor inductances can be decomposed in the mutual (L_{ad}, L_{aq}) and leakage inductances for each winding (L_{ls},L'_{lf},L'_{lD},L'_{lQ}):

$$L_d = L_{ad} + L_{ls} \quad (4)$$
$$L'_f = L_{ad} + L'_{lf} \quad (5)$$
$$L'_D = L_{ad} + L'_{lD} \quad (6)$$
$$L_q = L_{aq} + L_{ls} \quad (7)$$
$$L'_Q = L_{aq} + L'_{lQ} \quad (8)$$

In order to describe the complete system, the mechanical equation is presented with the following notations : p, the number of pole pairs, Γ_e, the electromagnetic torque, Γ_L the load torque, J, the total moment of inertia and f, the viscous friction coefficient.

$$J\frac{d\omega_e}{dt} + f.\omega_e = p.(\Gamma_e - \Gamma_L) \quad (9)$$
$$\Gamma_e = \frac{3}{2}p(\psi_d i_q - \psi_q i_d) \quad (10)$$

2.1 Taking into account magnetic saturation

Because of efficiency requirements, motor designers are optimising the mass versus loss trade-off. Therefore, the integrated starter generators are built to operate in high saturation mode resulting in a non-linear relation between the fluxes and currents, a complex phenomenon intensely studied for the last decades El-Serafi et al. (1988); El-Serafi and Abdallah (1992); Chedot et al. (2007).

The presented model is based on the hypothesis that the mutual inductances are constant and the cross-coupling terms are neglected between the inductances aligned on the $d-$axis, eq. (2), and those on the $q-$axis, eq. (3). There are several ways to take the saturation effect into account. In this work, a saturated flux model is obtained from the linear model by considering the inductances dependent on the currents circulating in the machine El-Serafi et al. (1988); El-Serafi and Abdallah (1992); Chedot et al. (2007). Therefore, the saturated d- and q- axis inductances are obtained by modifying their unsaturated values using a non-linear coefficient, K_{sat}, calculated on the basis of the equivalent magnetizing current i_m Maalouf et al. (2011). For simplifications reasons, the saturation factor is considered equal on both axis.

$$K_{sat} = f(i_m(i_d, i'_f, i_q)) \quad (11)$$

In this kind of representation, the leakage inductances have their magnetic paths in the air, therefore they are not affected by saturation El-Serafi et al. (1988). The mutual inductances have their magnetic paths in the body of the machine and will be affected by saturation (the overline marks a saturated parameter):

$$\overline{L_{ad}} = L_{ad}.K_{sat}$$
$$\overline{L_{aq}} = L_{aq}.K_{sat} \quad (12)$$

2.2 Simplified WRSM model at high frequency

In the perspective of a high frequency injection, a simplified model in the rotor reference frame of the stator voltage model from eq. (1) is possible. Expanding the flux expressions using eq. (2) and (3), the stator equations are written:

$$\begin{bmatrix} v_d \\ v_q \end{bmatrix} = \begin{bmatrix} R_s + \overline{L_d}.s & -\omega_e.\overline{L_q} \\ \omega_e.\overline{L_d} & R_s + \overline{L_q}.s \end{bmatrix} \begin{bmatrix} i_d \\ i_q \end{bmatrix} + \begin{bmatrix} \overline{L_{ad}}.s & -\omega_e.\overline{L_{aq}} \\ \omega_e.\overline{L_{ad}} & \overline{L_{aq}}.s \end{bmatrix} \begin{bmatrix} i'_D \\ i'_Q \end{bmatrix} + \begin{bmatrix} \overline{L_{ad}}.s \\ \omega_e.\overline{L_{ad}} \end{bmatrix} i'_f \quad (13)$$

Knowing that the carrier frequency of the injected signal is higher than the actual rotor angular velocity, $\omega_e << \omega_h$, the coupling terms dependent on the speed of the motor can be neglected for the HF-analysis.

$$\begin{bmatrix} v_d \\ v_q \end{bmatrix} = \begin{bmatrix} R_s + \overline{L_d}.s & 0 \\ 0 & R_s + \overline{L_q}.s \end{bmatrix} \begin{bmatrix} i_d \\ i_q \end{bmatrix} + \begin{bmatrix} \overline{L_{ad}}.s & 0 \\ 0 & \overline{L_{aq}}.s \end{bmatrix} \begin{bmatrix} i'_D \\ i'_Q \end{bmatrix} + \begin{bmatrix} \overline{L_{ad}}.s \\ 0 \end{bmatrix} i'_f \quad (14)$$

From the flux equations presented in (2) and (3), replaced in (1), the currents i'_f, i'_D, i'_Q could be expressed in function of i_d and i_q:

$$\begin{aligned} i'_f &= \frac{v'_f}{R'_f + L'_f.s} - \frac{\overline{L_{ad}}.s}{R'_f + L'_f.s} i_d - \frac{\overline{L_{ad}}.s}{R'_f + L'_f.s} i'_D \\ i'_D &= -\frac{\overline{L_{ad}}.s}{R'_D + L'_D.s} i_d - \frac{\overline{L_{ad}}.s}{R'_D + L'_D.s} i'_f \\ i'_Q &= -\frac{\overline{L_{aq}}.s}{R'_Q + L'_Q.s} i_q \end{aligned} \quad (15)$$

where s is the Laplace differential operator.

At standstill, under high frequency excitation, the field winding can be assimilated to a damper winding Rambetius and Piepenbreier (2014). Considering v'_f constant, an equivalent system model for very high frequencies, $(s = j\omega, \omega \to \infty)$, can be expressed using the HF-effective quantities :

$$\begin{bmatrix} v_{dh} \\ v_{qh} \end{bmatrix} = \begin{bmatrix} R_{d_{eff}} + L_{d_{eff}}.s & 0 \\ 0 & R_{q_{eff}} + L_{q_{eff}}.s \end{bmatrix} \begin{bmatrix} i_d \\ i_q \end{bmatrix} \quad (16)$$

The expressions of the effective resistances and inductances $R_{d_{eff}}$, $R_{q_{eff}}$, $L_{d_{eff}}$ and $L_{q_{eff}}$ are given by eq. (17) and eq. (18) respectively.

$$\begin{aligned} R_{d_{eff}} &= R_s + \frac{\left(\overline{L_{ad}} L'_{lD}\right)^2 R'_f + \left(\overline{L_{ad}} L'_{lf}\right)^2 R'_D}{\left(\overline{L_{ad}} L'_{lf} + \overline{L_{ad}} L_{ls} + L_{ls} L'_{lf}\right)^2} \\ R_{q_{eff}} &= R_s + \frac{\overline{L_{aq}}^2}{\left(\overline{L_{aq}} + L'_{lQ}\right)^2} R'_Q \end{aligned} \quad (17)$$

$$\begin{aligned} L_{d_{eff}} &= L_{ls} + \frac{\overline{L_{ad}} L'_{lD} L'_{lf}}{\overline{L_{ad}} L'_{lf} + \overline{L_{ad}} L_{ls} + L_{ls} L'_{lf}} \\ L_{q_{eff}} &= L_{ls} + \frac{\overline{L_{aq}} L'_{lQ}}{\overline{L_{aq}} + L'_{lQ}} \end{aligned} \quad (18)$$

Eq. (18) shows that effective inductance is dependent on the leakage inductances and less affected by saturation than the main magnetising inductance of one axis. This analytic form permits an evaluation of the effective inductances taking into account the saturation of the machine in order to analyse the feasibility of sensorless control. The stator winding resistance is also affected by the rotor parameters under high frequency excitations. Recent work suggests using the resistance saliency separately or together with the inductance saliency for sensorless control of AC machines Garca et al. (2011); Graus and Hahn (2015). The condition for saliency tracking methods for WRSM is adapted to:

$$\Delta R_{eff} = R_{d_{eff}} - R_{q_{eff}} \neq 0 \ or \quad (19)$$
$$\Delta L_{eff} = L_{d_{eff}} - L_{q_{eff}} \neq 0 \quad (20)$$

Equation (16) can be also described by two equivalent high frequency circuits for the two axis, represented in Fig. 1.

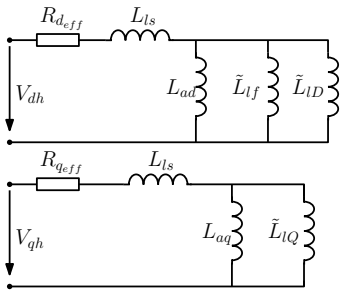

Fig. 1. Equivalent HF circuit for the d-axis (top figure) and for the q-axis (bottom figure)

2.3 Special case - no damping windings

When there are no damper windings, the case of a WRSM, the eq. (18) is:

$$L_{d_{eff}} = L_{ls} + \frac{\overline{L_{ad}} L'_{lf}}{\overline{L_{ad}} + L'_{lf}} \quad (21)$$
$$L_{q_{eff}} = L_{ls} + \overline{L_{aq}} \ \ (= L_q) \quad (22)$$

This result is also presented in Rambetius and Piepenbreier (2014), for the equivalent model in natural frame, with M_{af} the mutual inductance between the stator and rotor winding and L_f the rotor inductance in rotor frame. In this representation, it is easier to see that the direct main flux is naturally diminished by the rotor flux:

$$\begin{aligned} L_{d_{eff}} &= L_d - \frac{3}{2}\frac{M_{af}^2}{L_f} \\ L_{q_{eff}} &= L_q \end{aligned} \quad (23)$$

In the next section, the analytic expressions of the effective parameters are used in order to analyse the influence of the carrier frequency on the estimation errors.

3. PRINCIPLE OF HIGH FREQUENCY INJECTION

The rotating carrier injection consists in superimposing a balanced set of high frequency sinusoidal voltages to the reference voltages, outputs of the vector control:

$$\begin{bmatrix} V_{\alpha h} \\ V_{\beta h} \end{bmatrix} = V_h \begin{bmatrix} \cos(\omega_h t) \\ \sin(\omega_h t) \end{bmatrix} \quad (24)$$

Where ω_h and V_h are the pulsation and magnitude of the carrier signal respectively.

In order to extract the effect of the carrier frequency, the high frequency impedances of the machine are calculated. In eq. (16), the following notations are made : $R_{d_{eff}} + L_{d_{eff}}.s = Z_{dh}$ and $R_{q_{eff}} + L_{q_{eff}}.s = Z_{qh}$. Then, the stator currents in $\alpha\beta$ frame are obtained:

$$\begin{bmatrix} i_{\alpha h} \\ i_{\beta h} \end{bmatrix} = \begin{bmatrix} \Sigma Z + \Delta Z\cos(2\theta) & \Delta Z\sin(2\theta) \\ \Delta Z\sin(2\theta) & \Sigma Z - \Delta Z\cos(2\theta) \end{bmatrix}^{-1} \begin{bmatrix} V_{\alpha h} \\ V_{\beta h} \end{bmatrix} \tag{25}$$

Where $\Sigma Z = \frac{Z_{dh}+Z_{qh}}{2}$ and $\Delta Z = \frac{Z_{dh}-Z_{qh}}{2}$ are the average and differential inductance respectively. This simplified model can be used as starting point for both rotating and pulsating injection techniques.

Considering the HF voltage injection from eq. (24), in the measurement currents ($i_{\alpha\beta}$) we expect to find these three spectral components: a positive and a negative spectral component of the resulting HF-carrier currents along with the fundamental excitation spectral component at low frequency (where I_{fe} is the amplitude of the fundamental excitation):

$$i_{\alpha\beta} = \frac{V_h}{|Z_p|}e^{j(\omega_h t+\phi_p)} + \frac{V_h}{|Z_n|}e^{j(-\omega_h t+2\theta+\phi_n)} + I_{fe}e^{j(\omega_e t)} \tag{26}$$

$$Z_p = \frac{2Z_{dh}Z_{qh}}{Z_{dh}+Z_{qh}}, \quad Z_n = \frac{2Z_{dh}Z_{qh}}{Z_{dh}-Z_{qh}} \tag{27}$$

The phase noted by ϕ_p is the phase delay introduced by the high frequency impedance of the positive sequence, Z_p, and it will not influence the position information as this component is efficiently removed in the synchronous frame filtering.

The phase noted by ϕ_n is the phase delay introduced by the high frequency impedance of the negative sequence, Z_n, the component that contains spatial information in its phase. The amplitude of the negative sequence harmonic can be approximated to:

$$I_n = \frac{V_h}{|Z_n|} \approx \frac{V_h}{\omega_h}\frac{L_{d_{eff}} - L_{q_{eff}}}{2L_{d_{eff}}L_{q_{eff}}} \tag{28}$$

In order to validate this expression of the amplitude, a carrier signal of $V_h = 5V$ and $\omega_h = 800$Hz has been injected on the stator terminals of the studied machine. The complex frequency spectrum in the $\alpha\beta$-plane of the measured currents on the real machine is compared to the simulated machine in the same conditions.

Even though the analytical form of the amplitude is important in order to anticipate the Signal-to-Noise Ratio of the negative sequence Medjmadj et al. (2015), the exact value is not necessary in the estimation algorithm. The currents $i_\alpha\beta$ are in quadrature, so the current vector can be normalized in order to obtain the position dependent signals (see Fig. 4).

Because at high frequencies, the phase angle of the positive and the negative sequences (ϕ_p, ϕ_n) is $\frac{\pi}{2}$ for most of permanent magnet synchronous machines, it is common to take into consideration the phase angle introduced by the negative sequence in the injected signal:

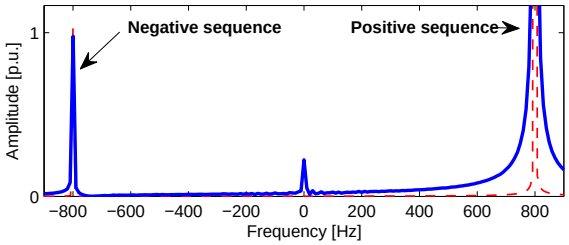

Fig. 2. Complex frequency spectrum for stator currents (red dotted line - simulation result, blue continuous line - real machine current spectrum)
The error between the two signal amplitudes is 5%.

$$\begin{bmatrix} V_{\alpha h} \\ V_{\beta h} \end{bmatrix} = V_h \begin{bmatrix} \cos(\omega_h t - \pi/2) \\ \sin(\omega_h t - \pi/2) \end{bmatrix} = V_h \begin{bmatrix} \sin(\omega_h t) \\ -\cos(\omega_h t) \end{bmatrix} \tag{29}$$

In this paper, eq. (24) is used because the phase angle is not $\frac{\pi}{2}$ under certain conditions further presented.

3.1 Consequences of the carrier frequency choice

The negative impedance transfer function describes the frequency response of the machine. Frequency dependent phase delays appear when one of the two poles of $\frac{1}{Z_n}$, situated at $\frac{R_{d_{eff}}}{L_{d_{eff}}}$ and $\frac{R_{q_{eff}}}{L_{q_{eff}}}$, is closer than one decade from the chosen carrier frequency. During operation, in presence of saturation and temperature variations, deviations from the nominal parameter's values occur and this will lead to evolutions of the frequency response of the machine.

For an accurate compensation, the saturation can been considered in the processing of the negative sequence phase, ϕ_n. Knowing that the saturation coefficient, K_{sat}, defined in eq. (11), is usually computed for to the torque control loop, it can be further used in order to compensate the effects of the magnetic saturation on the position estimation.

Variations of the stator resistance due to temperature dependency can also influence ϕ_n Reigosa et al. (2010). An illustration of carrier frequency phase delay taking into account both resistance and saturation variations is shown in Fig. 3.

Proposition for ϕ_n processing:

$$\begin{aligned} Z_{n_{sat}} &= -\frac{2(R_{d_{eff}} + L_{d_{eff}}.s)(R_{q_{eff}} + L_{q_{eff}}.s)}{\Delta R_{eff} + \Delta L_{eff}.s} \\ \phi_{n_{sat}} &= \arctan\left(Im\{Z_{n_{sat}}\}/Re\{Z_{n_{sat}}\}\right) \end{aligned} \tag{30}$$

It is worth mentioning that ϕ_n affects the double position information (2θ), so only half of the phase delay will be reflected on the estimated position.

As we can see in Fig. 3, the higher the injection frequency, the lower the carrier frequency induced errors and variations over the resistance uncertainty due to temperature evolution. However, the injection frequency is limited by the switching capacities of the inverter and the processing capacities of the signal processing modules.

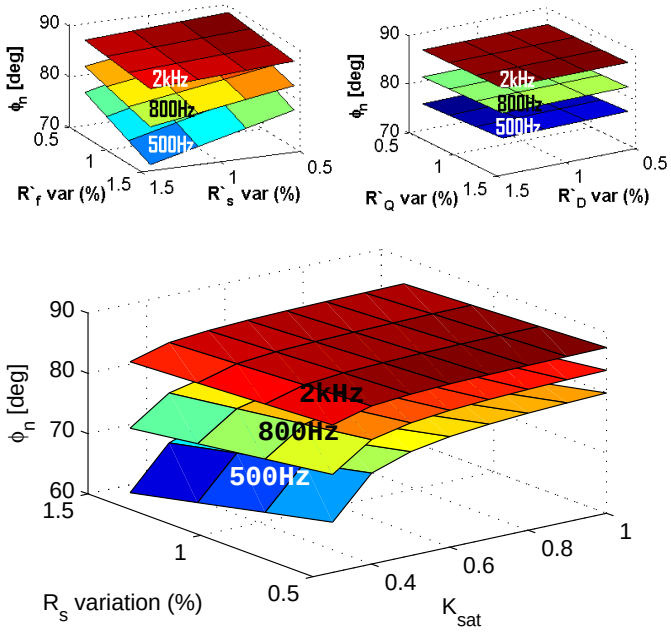

Fig. 3. Carrier frequency phase delay values taking into account parameters variations : left $\phi_n(R_s, R'_f)$, right $\phi_n(R'_D, R'_Q)$, bottom $\phi_n(R_s, K_{sat})$

3.2 Synchronous frame filtering of stator currents with phase compensation

The objective of the synchronous frame filtering is to extract the spatial informations contained in the phase of the negative-sequence carrier signal current and to deliver it to the observer. The synchronous frame filtering is presented in Fig. 4. The characteristics of the low pass filter (LP1) determine the bandpass and the noise attenuation on the estimated angle. For this considerations and implementation simplicity, the demodulation process with a 4th order low pass filter proposed in Mansouri-Toudert et al. (2013); Ovrebo (2004) is chosen for this paper.

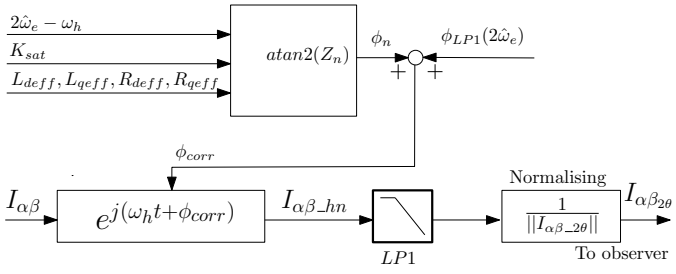

Fig. 4. Synchronous frame filtering with 4th order low-pass filter and phase compensation

The phase delays of the negative sequence (30) and that of the LP1 in the demodulation process can be analytically calculated. Without their compensation, the position estimation is affected. Mansouri-Toudert et al. (2013) propose to calculate the low-pass filtering bias in an adaptive way: based on the velocity estimation. It is then removed by subtraction from the output of the observer. The same approach can be used for the negative sequence phase delay. The compensation terms in Fig. 4 are:

$$\phi_{LP1} = \hat{\phi}(2\hat{\omega}_e)$$
$$\phi_n = \hat{\phi}_n(\omega_h - 2\hat{\omega}_e)$$

In the compensation scheme presented in Fig. 4, the phase delays are taken into consideration directly in the demodulation process by adding them to the first frequency translation operation. Therefore, the negative sequence present in $I_{\alpha\beta_{hn}}$ is moved around zero taking into account ϕ_n and anticipating the phase delay of the low pass filter, ϕ_{LP1}.

4. SPEED AND POSITION ESTIMATION

The inverse tangent function can be applied directly after the low pas filter in Fig. 4 in order to extract the position of the rotor. However, the PLLs, and the tracking observers are more robust towards measurement noise and allow the correction of the estimation errors.

A tracking observer makes use of the mechanical model of the machine, eq. 9, including load estimation, and offers the possibility to take into consideration the reference electromagnetic torque, Fig. (5). Initially, this tracking observers was used in order to reduce the effect of quantized angular resolution of velocity sensors in AC drives. In modern sensorless techniques, the input of the tracking observer is the estimated mechanical angle error: $\frac{1}{p}(\theta - \hat{\theta}) = \Delta\theta_m$, obtained by heterodyning of the demodulated signals, from Fig. 4.

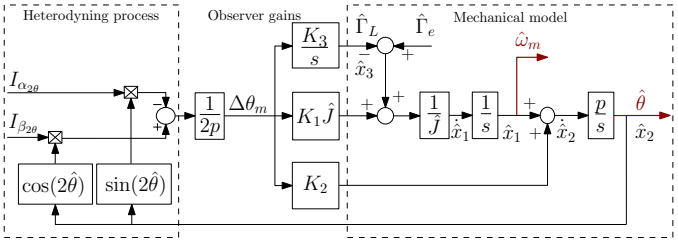

Fig. 5. Block diagram of the Luenberger tracking observer with the heterodyning operation

5. ILLUSTRATIVE EXAMPLE

In order to isolate the effect of the carrier frequency, the observer is simulated in open loop at standstill in Fig. 6. The results are obtained on a Matlab/SIMULINK nonlinear model of the brushless exciter starter/generator with the following characteristics: 35kVA, 115V, 400Hz, 3 Phases, Y connection and 3 pole pairs.

A carrier signal of $V_h = 15V$ and two carrier frequencies are compared (f_h = 500Hz and f_h = 2000Hz) for fixed saturation levels. The tracking observer was tuned for 200Hz bandwidth for the estimated position. A 4th order Butterworth low pass filter with 200Hz bandpass is used and its phase delay is compensated like Fig. 4.

The estimation error (in red) is different for each carrier frequency and corresponds to the phase delay of the negative impedance characterised in section II. The blue dotted line corresponds to the compensation algorithm

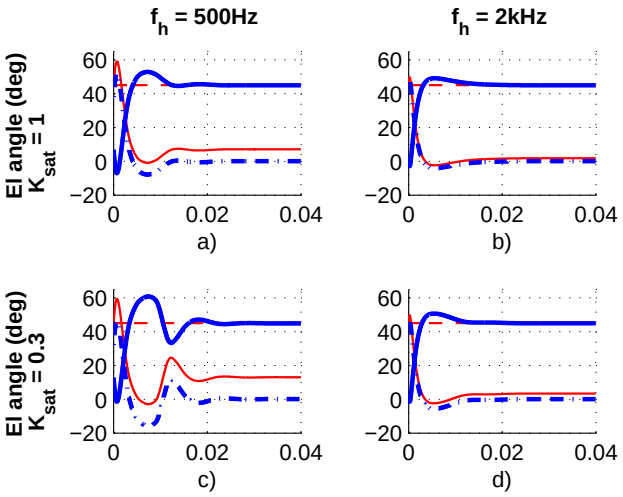

Fig. 6. Comparison of estimation errors in function of the carrier frequency and the saturation level. Blue continuous line - estimated angle with ϕ_n compensation, blue dotted line - estimation error with ϕ_n compensation, red dotted line - real position of the machine, red continuous line - position estimation without compensation

proposed in section III. We can observe that at higher carrier frequency, 2kHz, the estimation error is less important compared to the 500Hz case.

The authors are aware that the phase delay estimation requires good knowledge of the machine parameters and of the saturation characteristics, therefore, a reliable compensation may not always be possible. However, the results in this paper can be taken into account in the design phase of future machines in order to anticipate carrier frequency induced errors and to improve the saliency ratio for sensorless control purposes from the design phase.

6. CONCLUSION AND PERSPECTIVES

This paper has presented a high frequency model that highlights the saliency of a WRSM with dumper windings, based on the high frequency impedance of the machine. In order to better describe the HF-behaviour of the machine, the effective inductances and resistances have been calculated. The analytic expressions allow evaluations of the feasibility of sensorless control from the design phase of the machine.

Further, it has been shown that the negative sequence phase delay will introduce estimation errors that are dependent on the carrier frequency. Also, the errors introduced by parameter variations depend also on the carrier frequency: the lower the carrier frequency, the more important the effect of the parameter variation on the phase delay.

As the motor works in high saturation mode, an analytical form of the phase delay depending on the saturation level has been proposed. This analytical form is used in the proposed compensation scheme. The results show that the electrical angle estimation error is diminished and the overall performance is improved. However, further research work will concentrate on including the cross-saturation effect in the model. Experimental measurements of the effective inductances is going to be conducted on a test bench. A complete description of the phase delay ϕ_n will allow further improvements of the high frequency model and simplified compensation.

REFERENCES

Barakat, A., Tnani, S., Champenois, G., and Mouni, E. (2010). Analysis of synchronous machine modeling for simulation and industrial applications. *Simulation Modelling Practice and Theory*, 18(9), 1382–1396.

Briz, F., Diez, A., and Degner, M. (2000). Dynamic operation of carrier-signal-injection-based sensorless direct field-oriented ac drives. *Industry Applications, IEEE Transactions on*, 36(5), 1360–1368. doi: 10.1109/28.871285.

Chedot, L., Friedrich, G., Biedinger, J.M., and Macret, P. (2007). Integrated starter generator: The need for an optimal design and control approach. application to a permanent magnet machine. *IEEE Transactions on Industry Applications*, 43(2), 551–559. doi: 10.1109/TIA.2006.889900.

Choi, J., Jeong, I., Nam, K., and Jung, S. (2013). Sensorless control for electrically energized synchronous motor based on signal injection to field winding. In *Industrial Electronics Society, IECON 2013 - 39th Annual Conference of the IEEE*, 3120–3129. doi: 10.1109/IECON.2013.6699627.

El-Serafi, A.M. and Abdallah, A.S. (1992). Saturated synchronous reactances of synchronous machines. *IEEE Transactions on Energy Conversion*, 7(3), 570–579. doi: 10.1109/60.148580.

El-Serafi, A.M., Abdallah, A.S., El-Sherbiny, M.K., and Badawy, E.H. (1988). Experimental study of the saturation and the cross-magnetizing phenomenon in saturated synchronous machines. *IEEE Transactions on Energy Conversion*, 3(4), 815–823. doi:10.1109/60.9357.

Garca, P., Briz, F., Reigosa, D., Blanco, C., and Guerrero, J.M. (2011). On the use of high frequency inductance vs. high frequency resistance for sensorless control of ac machines. In *2011 Symposium on Sensorless Control for Electrical Drives*, 90–95. doi: 10.1109/SLED.2011.6051550.

Garcia, P., Briz, F., Degner, M.W., and Diaz-Reigosa, D. (2006). Accuracy and bandwidth limits of carrier signal injection-based sensorless control methods. In *Conference Record of the 2006 IEEE Industry Applications Conference Forty-First IAS Annual Meeting*, volume 2, 897–904. doi:10.1109/IAS.2006.256631.

Graus, J. and Hahn, I. (2014). Modelling and optimization of a short-circuited rotor winding of a pmsm for saliency tracking. In *2014 IEEE 5th International Symposium on Sensorless Control for Electrical Drives*, 1–8. doi: 10.1109/SLED.2014.6844971.

Graus, J. and Hahn, I. (2015). Improved accuracy of sensorless position estimation by combining resistance- and inductance-based saliency tracking. In *Industrial Electronics Society, IECON 2015 - 41st Annual Conference of the IEEE*, 002886–002891. doi: 10.1109/IECON.2015.7392540.

Griffo, A., Drury, D., Sawata, T., and Mellor, P. (2012). Sensorless starting of a wound-field synchronous starter/generator for aerospace applications. *Industrial*

Electronics, IEEE Transactions on, 59(9), 3579–3587. doi:10.1109/TIE.2011.2159953.

Kato, Y. and Nishikata, S. (2009). Studies on a sensorless starting method for self-controlled synchronous motors without damper windings. In *2009 International Conference on Electrical Machines and Systems*.

Koteich, M., Maloum, A., Duc, G., and Sandou, G. (2015). Observability analysis of sensorless synchronous machine drives. In *14th annual European Control Conference - ECC 2015*. Linz, Austria.

Maalouf, A., Idkhajine, L., Le Ballois, S., and Monmasson, E. (2011). Field programmable gate array-based sensorless control of a brushless synchronous starter generator for aircraft application. *Electric Power Applications, IET*, 5(1), 181–192.

Mansouri-Toudert, O., Zeroug, H., Auger, F., and Chibah, A. (2013). Improved rotor position estimation of salient-pole pmsm using high frequency carrier signal injection. In *Mechatronics (ICM), 2013 IEEE International Conference on*, 761–767. IEEE.

Markunas, A.L. and Romenesko, C.J. (2006). Brushless wound field synchronous machine rotor position tracking with exciter stator current harmonic tracking. US Patent 7,132,816.

Medjmadj, S., Diallo, D., Mostefai, M., Delpha, C., and Arias, A. (2015). Pmsm drive position estimation: Contribution to the high-frequency injection voltage selection issue. *IEEE Transactions on Energy Conversion*, 30(1), 349–358. doi:10.1109/TEC.2014.2354075.

Ovrebo, S. (2004). *Sensorless control of permanent magnet synchronous machines*. Ph.D. thesis, Dept. Elect. Power Eng., Norwegian Univ. Sci. Technol. (NTNU), Trondheim, Norway.

Raca, D., Garcia, P., Reigosa, D., Briz, F., and Lorenz, R. (2008). A comparative analysis of pulsating vs. rotating vector carrier signal injection-based sensorless control. In *Applied Power Electronics Conference and Exposition, 2008. APEC 2008. Twenty-Third Annual IEEE*, 879–885. doi:10.1109/APEC.2008.4522824.

Rambetius, A., Luthardt, S., and Piepenbreier, B. (2014). Modeling of wound rotor synchronous machines considering harmonics, geometric saliencies and saturation induced saliencies. In *2014 International Power Electronics Conference (IPEC-Hiroshima 2014 - ECCE ASIA)*, 3029–3036. doi:10.1109/IPEC.2014.6870116.

Rambetius, A. and Piepenbreier, B. (2014). Comparison of carrier signal based approaches for sensorless wound rotor synchronous machines. In *Power Electronics, Electrical Drives, Automation and Motion (SPEEDAM), 2014 International Symposium on*, 1152–1159. doi: 10.1109/SPEEDAM.2014.6871919.

Reigosa, D.D., Garcia, P., Briz, F., Raca, D., and Lorenz, R.D. (2010). Modeling and adaptive decoupling of high-frequency resistance and temperature effects in carrier-based sensorless control of pm synchronous machines. *IEEE Transactions on Industry Applications*, 46(1), 139–149. doi:10.1109/TIA.2009.2027640.